Fabrication of Silver Nanoparticle-Embedded Polymer Promoted by Combined Photochemical Properties of a 2,7-Diaminofluorene Derivative Dye

Lavinia Balan,* Ming Jin, and Jean-Pierre Malval*

Département de Photochimie Générale, UMR CNRS 7525, Université de Haute Alsace, ENSCMu. 3 rue Alfred Werner, 68093 Mulhouse, France

Hélène Chaumeil and Albert Defoin

Laboratoire de Chimie Organique et Bioorganique, UMR CNRS 7015, Université de Haute Alsace, ENSCMu. 3 rue Alfred Werner, 68093 Mulhouse, France

Loïc Vidal

Institut de Chimie de Surface et Interface, UPR CNRS 9069, 15 rue Jean Starcky, 68093 Mulhouse, France

Received August 6, 2008; Revised Manuscript Received October 8, 2008

ABSTRACT: A one step method for the fabrication of silver nanoparticle-embedded polymer is detailed from the mechanistic aspects to the structural analysis of the material. A 2,7-diaminofluorene derivative is employed both as a photoreductant agent of silver precursors and as a free radical photoinitiator to produce silver nanoparticles in a poly(ethylene glycol) matrix at the same time. Each photophysical mechanism is separately investigated and quantified by steady state and time-resolved spectroscopy. The analysis confirms the key role the dye radical cation in the photopolymerization. Moreover, the addition of an amine co-initiator induces a clear acceleration of the photopolymerization rate and leads to a new distinctive mechanism. As a consequence, the morphology of the resultant silver nanocomposite exhibits different size distributions characterized by transmission electron microscopy. This structural observation was also correlated by an unexpected metal-enhancement fluorescence process arising from residual dyes entrapped in the metal−polymer.

Introduction

Research in novel methods to prepare metal nanocomposite materials has been greatly stimulated due to their attractive properties that lead to a large set of promising applications in optics,[1,2] magnetics, microelectronics,[3,4] and solar energy conversion.[5,6] One of the main interests of metal nanoparticles stems from their unique physical properties, which can be addressed by the chemical control of their shape and size.[7−9] For instance, silver nanoparticles with spherical shape and nanometer size exhibit a very intensive absorption band in the visible region due to their surface plasmon resonance. The absorption coefficient can be orders of magnitude larger than strongly absorbing organic chromophores. Besides, the enhanced electromagnetic fields generated in the close-proximity of the metal surface have a strong influence on the local environment which is illustrated by surface-enhanced Raman scattering[10,11] (SERS) or by metal-enhanced fluorescence (MEF) process.[6,12−14] Nanocomposite materials combine together the different properties of components. However, to maintain these high performances mainly relies on the homogeneous dispersion of uniformly shaped and sized particles into the matrix. Generally, metal−polymer nanocomposites are obtained via multistep methods. The silver nanoparticles which are first produced from the reduction of silver precursors are then dispersed into a polymer matrix to obtain a self-assembly functionalized structure.[15] However, this "ex situ" method is limited by difficulty to control the particles monodispersity over a large scale.[16−18] In the "in situ" methodology, the metal nanoparticles are produced in the polymer from cationic precursors that exhibit a better dispersion ability and that undergo a facile chemical[19,20] or photochemical reduction.[21−24] The photoreduction is often promoted by dyes embedded in the polymer or present in the chemical structure of the matrix. However, few examples have been devoted to enlarge the role of this chromophore by combining its photoreduction ability with its propensity to photoinitiate a polymerization reaction.

In this present report, we describe a detailed strategy to produce a nanoparticles-embedded polymer through a photoinduced one-step method. This method relies on the complementary properties of a 2,7-diaminofluorene derivative (Scheme 1), which acts both as photoreductant and as photoinitiator. After an insight analysis of the photophysical features of the chromophore, both mechanistic aspect of the sequential photoreactions and structural description of the obtained nanomaterials are investigated.

Experimental Section

Material. All the solvents employed for photophysical analysis were Aldrich or Fluka spectroscopic grade. The silver nitrate ($AgNO_3$), the copper(II) sulfate ($CuSO_4$), and *N*-methyl diethanolamine (MDEA) were purchased from Aldrich. Polyethylene glycol diacrylate monomer (SR344, $M_w = 508$ g mol^{-1}) was provided by Sartomer.

Synthesis of 9,9-Didecyl-*N*^{2},*N*^{7}-bis(4-methoxyphenyl)-*N*^{2},*N*^{7}-diphenyl-9*H*-fluorene-2,7-diamine (DAF). 2,7-Dibromo-9,9-didecyl-9*H*-fluorene (3.0 g, 5.0 mmol), *N*-(4-methoxyphenyl)aniline (2.15 g, 10.8 mmol), and potassium *tert*-butoxide (2.0 g, 17.8 mmol) were first mixed together under an argon atmosphere, 100 mL of dry toluene is then injected prior addition of $Pd_2(dba)_3$ (91.5 mg, 0.1 mmol). Tri-*tert*-butylphosphine (50 mg, 0.25 mmol) in 1 mL of dry toluene is finally syringed and the mixture was stirred

* To whom correspondence should be addressed. E-mail: lavinia.balan@uha.fr (L.B.); jean-pierre.malval@uha.fr (J.-P.M.).

10.1021/ma8017926 CCC: $40.75
Published on Web 11/06/2008

Scheme 1. Molecular Structure of DAF

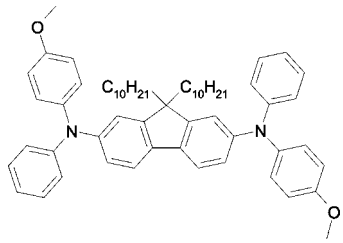

overnight in 70 °C oil bath. The mixture was then allowed to cool to room temperature and first filtered under silica gel to get rid of the catalyst and salt using toluene as eluent. After concentration under vacuum, the residue was purified by silica gel chromatography (9:1, cyclohexane and ethyl acetate). Yield 85%. ^{1}H NMR (C_6D_6, 400 MHz, 295 K): 0.90 (t, J = 7.2 Hz, 6 H), 0.93 (m, 4 H), 1.10 (m, 8 H), 1.24 (m, 20 H), 1.69 (m, 4 H), 3.30 (s, 6 H), 6.74 (d, J = 6.8 Hz, 4 H), 6.86 (t, J = 7.2 Hz, 2 H), 7.13−7.17 (m, 10 H), 7.27 (d, J = 7.8 Hz, 4 H), 7.34 (d, J = 1.6 Hz, 2 H), 7.39 (d, J = 8.3 Hz, 2 H). ^{13}C NMR (C_6D_6, 100.6 MHz, 295 K): 14.4, 23.1, 24.6, 29.8, 29.9, 30.1, 30.2, 30.6, 32.4, 40.5, 55.0, 55.3, 115.2,118.6, 120.3, 122.0, 123.0, 123.2, 127.3, 129.5, 136.3, 141.6, 147.5, 149.2, 152.5, 156.7. IR (KBr): 695, 749, 819, 830, 1039, 1180, 1242, 1269, 1314, 1440, 1466, 1494, 1507, 1594, 2852, 2925 cm^{-1}. HRMS, ESI-MicroTOF, calcd for $C_{59}H_{72}N_2O_2$, M^+, 840.5594; found, 840.5671.

General Techniques. The absorption measurements were carried out with a Perkin-Elmer Lambda 2 spectrometer. Steady-state fluorescence and phosphorescence spectra were collected from a FluoroMax-4 spectrofluorometer. Emission spectra are spectrally corrected, and fluorescence quantum yields include the correction due to solvent refractive index and were determined relative to quinine bisulfate in 0.05 molar sulfuric acid (ϕ = 0.52).[25]

The fluorescence lifetimes were measured using a Nano LED emitting at 372 nm as an excitation source with a nano led controller module, Fluorohub from IBH, operating at 1 MHz. The detection was based on an R928P type photomultiplier from Hamamatsu with high sensitivity photon-counting mode. The decays were fitted with the iterative reconvolution method on the basis of the Marquardt/Levenberg algorithm.[26] Such a reconvolution technique allows an overall-time resolution down to 0.15 ns. The quality of the exponential fits was checked using the reduced χ^2 ($\leq$1.2).

Phosphorescence and steady-state anisotropy measurements were performed in ethanol at 77 K. The samples are placed in a 5-mm diameter quartz tube inside a Dewar filled with liquid nitrogen.

Laser flash photolysis at nanosecond time scale was carried out with an Edinburgh Analytical Instruments LP900 equipped with a 450-W pulsed Xe arc lamp, a Czerny-Turner monochromator and a fast photomultiplier. The samples were irradiated with the third harmonic (λ = 355 nm, ~10 ns, 5 mJ per pulse) of a Nd/YAG Powerlite 9010 from Continuum. The sample was purged with nitrogen for 15 min prior to photophysical studies.

The cyclic voltammetry experiments (using a computer-controlled Princeton 263A potentiostat with a three-electrode single-compartment cell; a saturated calomel electrode in methanol used as a reference was placed in a separate compartment) were performed at 300 K, in Ar-degassed acetonitrile with a constant concentration (0.1 M) of n-Bu_4BF_4. Ferrocene was used as an internal reference.

The resin formulation, typically DAF (0.5 wt %), MDEA (1 wt %), and $AgNO_3$ (1 wt %) in monomer, is sandwiched between two glass plates with a calibrated thickness wedge assuring a constant optical path length of 16 μm. Photochemical reactions were carried out under irradiation at 375 nm with a laser diode from (Cube type from Coherent). The progress of the reaction was monitored via UV−vis absorption spectra.

The photopolymerization was monitored in situ by real-time Fourier transformed infrared spectroscopy with an AVATAR 360 FTIR spectrometer from Nicolet. The laminated formulation sandwiched between two polypropylene film (10 μm thick), deposited on a BaF_2 pellet, were irradiated at 365 nm with Xe-lamp source (LC5 8253 from Hamamatsu) equipped with interferometer filter. The conversion rates are obtained from the disappearance of the progressive vinyl C=C stretching vibration band at 1630 cm^{-1}.

Transmission electron microscopy (TEM) is used to characterize the size and shape of Ag nanoparticles. The nanocomposites were cut by means of a microtome (LKB model 8800) and placed on the observation grid to get their TEM images. Transmission electron microscopy measurement is carried out at 200 kV using a Philips CM20 instrument with Lab6 cathode.

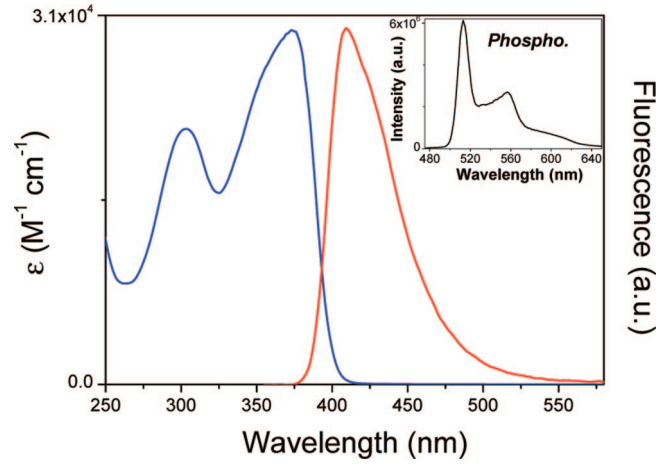

Figure 1. Absorption and normalized fluorescence spectra of **DAF** (solvent: acetonitrile). Inset: Time-gated phosphorescence spectrum of **DAF** in glassy matrix of ethanol (delay: 0.5 s).

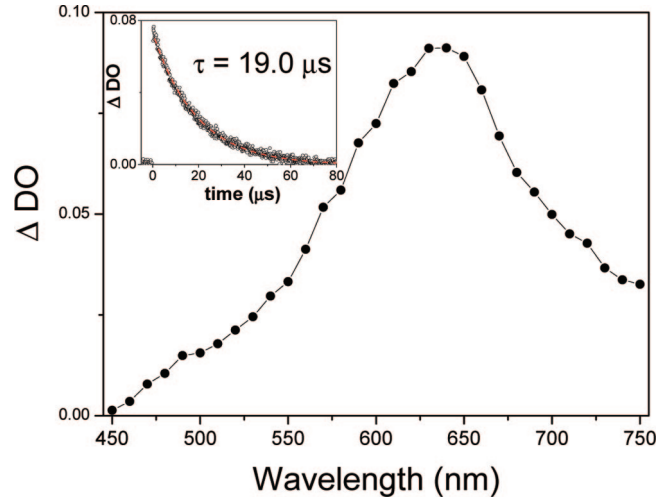

Figure 2. Transient absorption spectrum of **DAF** collected in oxygen free acetonitrile (1.1 μs after 355 nm laser pulse). Inset: decay of the transient at 630 nm.

Results and Discussion

Photophysical and Electronic Properties of DAF. Figure 1 depicts the absorption and the fluorescence spectra of **DAF** in acetonitrile. The absorption spectrum displays two main bands with maximum wavelengths at 305 and 375 nm respectively. The extinction coefficient at the maximum absorption has a value of about 29800 M^{-1} cm^{-1}. The fluorescence band which exhibits a maximum at 410 nm is mirror image of the last absorption band. This fluorescence spectrum is slightly sensitive to solvent polarity, consistent with a weak polar character of

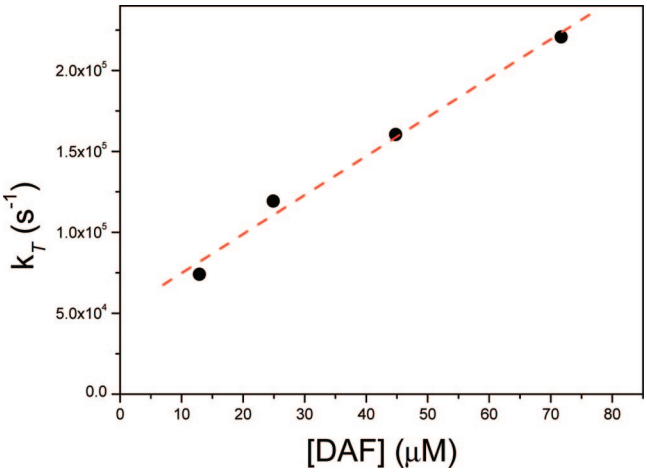

Figure 3. Dependence of pseudofirst-order decay rate constant of triplet chromophore on concentration of the dye in acetonitrile.

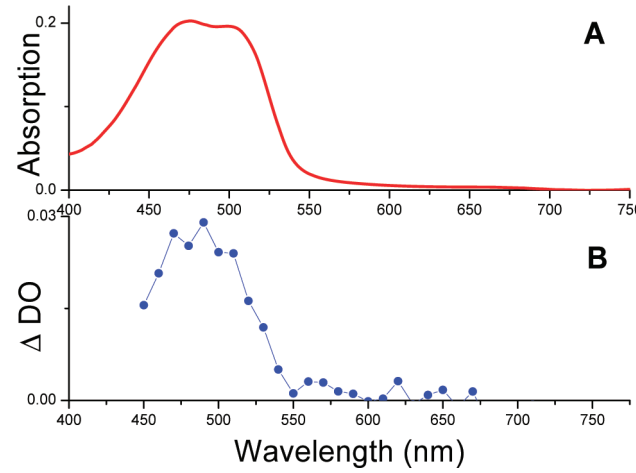

Figure 4. Comparison of the stationary absorption spectrum of **DAF**$^{\bullet+}$ (A) with the transient spectrum of **DAF** (B) in acetonitrile (20 μs after laser pulse, [DAF] = 7 × 10^{-5} M).

the excited state.[27−29] The emission quantum yield of **DAF** is about 0.52 in acetonitrile and the analysis of fluorescence decay shows a monoexponential character with a lifetime of 1.56 ns. The 0−0 transition energy measured from the intercept of normalized absorption and fluorescence spectra has a value of ca. 3.18 eV. The phosphorescence spectrum is located in the 500−650 nm range with a maximum emission at 515 nm which leads to a triplet energy of about 2.41 eV (inset of Figure 1). The chromophore has a phosphorescence lifetime of about 1.5 s, which suggests a $\pi-\pi^*$ character for T_1 state. The transient absorption spectra of **DAF** (5 × 10^{-6} M) were recorded after laser excitation at 355 nm in deaerated acetonitrile. Figure 2 shows the T_1-T_n spectrum of **DAF** (^{3}**(DAF)***), it exhibits an intensive band centered at 630 nm. The kinetic decay of this band follows a first-order kinetics, with a lifetime of about 19 μs (inset of Figure 2). The transient observed upon **DAF** photolysis in acetonitrile is quenched by oxygen with a high rate constant of about 1.6 × 10^{10} M^{-1} s^{-1}, which suggests a diffusion-controlled reaction.

The triplet lifetime is also dependent upon ground-state dye concentration. Such a dependence is an indication of a self-quenching process according to the following reactions:

$$^3(\mathrm{DAF})^* + \mathrm{DAF} \rightarrow \mathrm{DAF} + \mathrm{DAF}$$
$$^3(\mathrm{DAF})^* + \mathrm{DAF} \rightarrow \mathrm{DAF}^{\bullet+} + \mathrm{DAF}^{\bullet-}$$

The global bimolecular quenching rate constant for the quenching of ^{3}**(DAF)*** by ground-state chromophore was determined by measuring the pseudofirst-order decay rate constants of the triplet (k_T) at various concentrations of **DAF** from 5 × 10^{-6} M to 5 × 10^{-5} M. The linear dependence of k_T upon dye concentration is shown in Figure 3. The quenching rate constant determined from the slope of this plot exhibits a high value of 2.4 × 10^9 M^{-1} s^{-1}. Consecutive to the quenching of the triplet state, the transient absorption spectrum shows the concomitant development of a new band located in the 450−550 region. This new band which corresponds to the absorption of a long-lived species is ascribable to the radical cation of **DAF** (**DAF**$^{\bullet+}$). Indeed, such a persistent radical can be easily obtained from a stoechiometric reaction between $CuSO_4$ salt and the chromophore in acetonitrile. This redox reaction[30,31] is only possible if the aryl amine reductant has an oxidation potential (E_{ox}) below 1 V versus SCE. In the case of **DAF**, the oxidation potential, measured by cyclic voltammetry, has a value of 0.55 V versus SCE in acetonitrile in good accordance with literature.[32] Figure 4 shows a comparison between the stationary absorption spectrum of **DAF**$^{\bullet+}$ with the transient absorption one

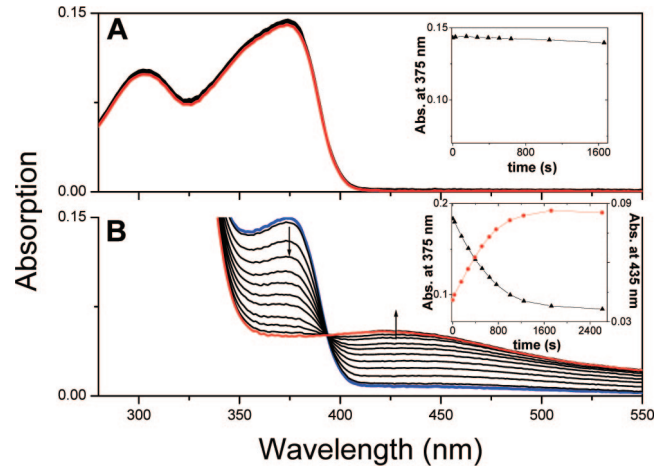

Figure 5. Evolution of the absorption spectra of **DAF** (5 × 10^{-6} M) in presence of $AgNO_3$ (0.1 M) in acetonitrile upon irradiation at 375 nm. (A) Reference sample without silver salt (inset: kinetics at 375 nm). (B) Mixed solution of dye with silver cations (inset: kinetics monitored at 375 and 435 nm).

obtained from a high concentrated solution of the chromophore. Both spectra match very well and thus confirm the photochemical production of radical cations. However, the radical anion was not detected within nanosecond time range, this should be ascribed to the very short-time living character of this rich electron transient species.

Photoreduction Mechanism of Ag^+ by DAF. Figure 5 shows the evolution of the absorption spectrum of a solution of **DAF** (5 × 10^{-6} M) mixed with a large excess of $AgNO_3$ (0.1 M) in acetonitrile, this solution is then irradiated at 375 nm. A reference sample without silver nitrate is used for comparison. While the absorption spectrum of the reference remains totally invariant upon irradiation, the last absorption band of **DAF** is progressively collapsing in presence Ag^+. No recovery of the absorption bands of **DAF** was observed after irradiation which confirms the irreversible character of the phototransformation. Consecutive to the bleaching of **DAF**, a new broadband with a maximum wavelength at 425 nm is developing. The presence of an isosbestic point at 393 nm indicates the occurrence of an equilibrium reaction. Such a band corresponds, for a large part, to the surface plasmon band of silver nanoparticles produced from a photoreduction of Ag^+ by excited states of the dye. Silver nanoparticles obtained upon the photoreduction are not stable in solution since the surface

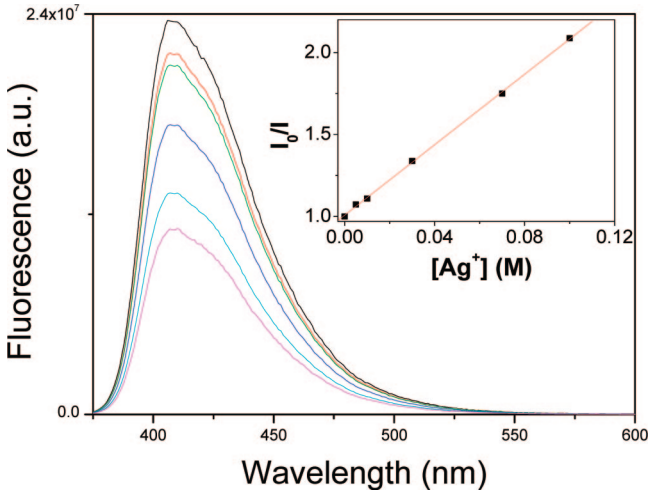

Figure 6. Fluorescence quenching of **DAF** upon increasing amount of $AgNO_3$ (λ_{exc} = 355 nm; solvent, acetonitrile). Inset: corresponding Stern−Volmer plot.

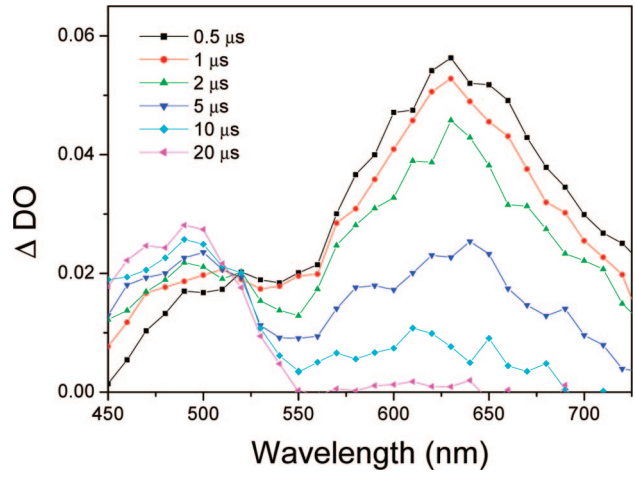

Figure 7. Time-resolved transient absorption spectra of **DAF** (5×10^{-6} M) mixed with $AgNO_3$ (0.1 M) in oxygen-free acetonitrile recorded at various times after 355 nm laser pulse excitation.

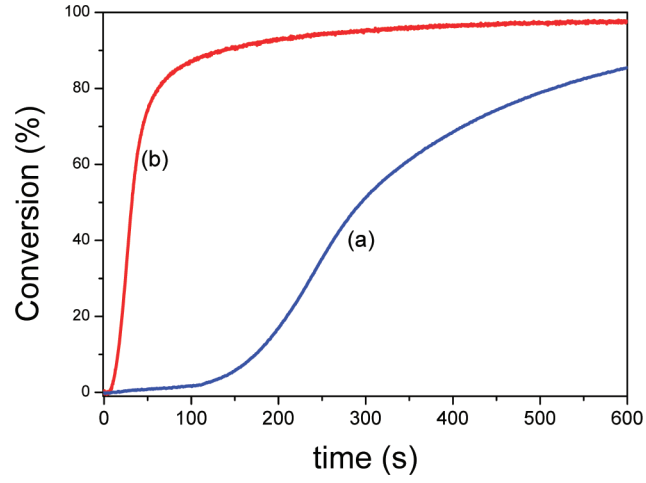

Figure 8. Real-time FTIR kinetics conversion curves for UV-curing at 365 nm of resins with (a) **DAF**, 0.5 wt %; and with (b) **DAF**/MDEA, 0.5 wt %/1 wt %.

plasmon band is progressively decreasing and shifting to the red region which is an indication of particles aggregation.

Upon excitation of **DAF**, singlet and triplet excited states are generated and can induce electrons transfer reactions in presence of Ag^+. In both cases, the driving forces for the photoinduced electron transfer (PET) reaction, as estimated from the Rehm−Weller equation ($\Delta G = E_{ox} - E_{red} - E_{ex}$), neglecting the Coulomb part of the stabilization energy is largely exergonic with values of about −3.18 eV for a PET from the singlet state and about −2.41 eV from the triplet one.

As shown in Figure 6, the addition of $AgNO_3$ to a solution of **DAF** in acetonitrile leads to the quenching of its fluorescence emission. The ratio of the maximum fluorescence intensities before and after the addition of Ag^+ was fit to following equation

$$\frac{I_0}{I} = 1 + K_{SV}[Ag^+]$$

Linear regression analysis of the plots (inset of Figure 6) yields a Stern−Volmer constant (K_{SV}) of 10.9 M^{-1}. According to the decrease of the fluorescence lifetime of **DAF** in presence of Ag^+, a dynamic quenching is clearly occurring with a rate constant of about 7.0×10^9 M^{-1} s^{-1}.

In the same manner, a progressive decrease of the triplet lifetime is observed in presence of increasing amount of silver cation. In this case, the bimolecular quenching rate of the reaction is only 2.1×10^6 M^{-1} s^{-1}. However, the evolution of transient absorption spectra, displayed in Figure 7, clearly shows the progressive growth the radical cation band ($\lambda_{max} \sim 490$ nm) consecutive to the decrease of the triplet absorption one. Besides, the decrease of the transient lifetime upon increasing Ag^+ concentration is accompanied by a first-order growth monitored at 490 nm. Hence, the generation of radical cation is correlated to the consumption of **^{3}(DAF)***, which confirms that PET process mainly derives from the triplet state.

This dye, which exhibits a photoreduction ability of silver cation, can also induce free-radical polymerization, whose mechanism will be detailed in the next paragraph.

Photoinitiating Ability of DAF. The dye is directly mixed to a poly(ethylene glycol) diacrylate monomer and the laminated film of this formulation is irradiated under excitation at 365 nm. The extent of polymerization is monitored by a real-time FT-IR technique, the conversion rate of acrylate double bonds is shown in figure 8. Upon irradiation, an induction time is first observed. It corresponds to the inhibition of the triplet state of **DAF** by residual oxygen which is consistent with the high oxygen sensibility of the excited species previously quantified. This inhibition time can be drastically reduced upon increasing the irradiance of the excitation source: increasing the irradiance from 9 to 18 mW·cm^{-2} leads to a decrease of the induction time from 112 to 30 s. After total consumption of oxygen, the conversion rate undergoes a clear acceleration and reaches a conversion of 80% after 600 s irradiation. The mechanism of the photoinitiation process should imply the key role of the radical cation initially generated from the triplet self-quenching reaction. This hypothesis is supported by the concentration effect of the dye which strongly affects the initial rate of polymerization. Moreover the addition of the monomer induces a significative decrease of the lifetime of **DAF$^{\bullet+}$** during photolysis experiment, whereas the lifetime of triplet state remains totally invariant. Therefore, we propose that the quenching of radical cation in presence of monomer is ascribable to a hydrogen atom abstraction reaction from the poly(ethylene glycol) monomer. This reaction should be sequentially described by a first electron transfer from the monomer to **DAF$^{\bullet+}$** followed by a proton transfer process which produces a α-oxyalkyl radical and the protonated chromophore as follows

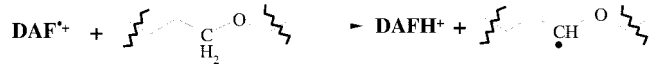

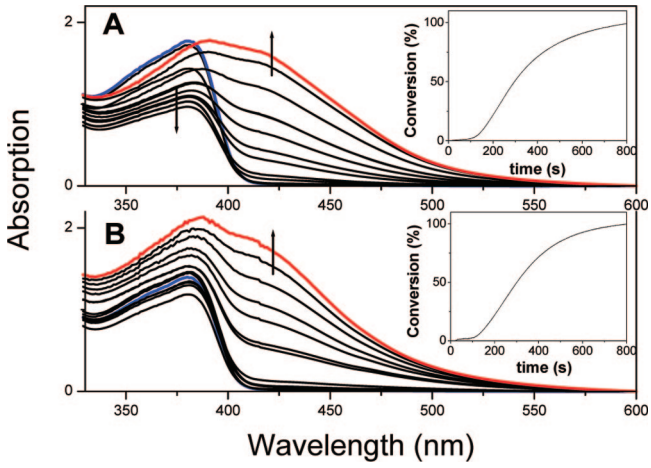

Figure 9. Growth of absorption spectrum of silver nanoparticles during photopolymerization ($\lambda_{exc} = 375$ nm). (A) Formulation **DAF**/$AgNO_3$, 0.5 wt %/1 wt %; (B) Formulation **DAF**/$AgNO_3$/MDEA, 0.5 wt %/1 wt %/1 wt %. Insets: corresponding real-time FTIR conversion curves.

The propensity to abstract H-atom from the monomer has already been described for photoinitiating systems as excited maleimide in presence of vinyl ether[33] or excited camphorquinone in presence of triethylene glycol dimethacrylate monomer.[34−36] Besides the hydrogen abstractability of nitrogen-centered radical cations was also demonstrated for acridine cations[37] or for unsaturated amine radical cations.[38] The subsequent addition of the α-oxyalkyl radical onto the acrylate monomer double bond should initiate the polymerization. However, steric effect of repulsion between the crowded radical and the alkene substituents should decrease the rate constant of addition.[39]

As shown in Figure 8, the addition to the formulation of a co-initiator as the *N*-methyl diethanolamine (MDEA) strikingly increases the initial polymerization rate by a factor 10 and 80% of conversion is achieved after 80 s irradiation. In this case, the mechanism is somewhat different because the hydrogen abstraction mainly occurs from MDEA (hydrogen donor) and leads to the production of an α-aminoalkyl radical whose reactivity upon addition reaction onto acrylate double bond should be more efficient as a long hindered α-oxyalkyl radical.[39,40]

Hence, **DAF** appears as an intrinsic photoinitiator for free radical polymerization. When associated to a hydrogen donor, a substantial improvement of the polymerization rate is clearly evidenced. The combination of these photoinitiating properties with the ability of the chromophore to generate silver nanoparticles through a PET process lead us to describe a one-pot method to produce a silver-acrylate nanocomposite.

Fabrication of Silver Nanoparticle Embedded Polymer. Figure 9A depicts the time evolution of the absorption spectrum relative to a formulation where the dye (0.5 wt %) and the silver nitrate salt (1 wt %) are mixed together in the diacrylate resin, the formulation is then continuously irradiated at 375 nm. As previously observed in solution, the silver plasmon band strongly develops in the 350−550 nm region with a maximum located at ∼420 nm. The transparent film turns yellow in color as a function of irradiation time. In the same manner, the absorption band of the dye is progressively decreasing, however its overlap with the absorption the silver nanoparticles excludes any further analysis of the surface plasmon resonance. The kinetics of monomers conversion monitored by time-resolved FT-IR spectroscopy exhibits the same profile as that obtained from the formulation without $AgNO_3$ (inset of Figure 9A). This indicates that both photoreactions (i.e., cations photoreduction and photoinitiation) occur during parallel processes that do not interfere with each other. According to the comparison of their respective reaction rate constants measured in acetonitrile, the triplet state self-quenching process is 1000 times more efficient as the Ag^+ photoreduction. Hence, the occurrence of the photoreduction clearly constitutes a minor deactivation pathway of the triplet state which is consistent with the invariance of the kinetics profile. The addition of MDEA to this formulation also leads to the surface plasmon band as shown in Figure 9B. However, in this case, the absorption band of the dye remains invariant during irradiation and, surprisingly, we can observe that the photopolymerization kinetics profile does not matches anymore the kinetics relative to the formulation with MDEA shown in Figure 8. Indeed, the presence of Ag^+ leads to a strong decrease of the photopolymerization rate due to a competing reduction of metal cation by the α-aminoalkyl radical. In this case, the silver nanoparticles are meanly provided from the following sequential reactions

$$DAF^{\bullet+} + MDEA \rightarrow DAFH^+ + MDEA^{\bullet}$$
$$MDEA^{\bullet} + Ag^+ \rightarrow MDEA^+ + Ag_0$$

Hence, the electron transfer rate constant from α-aminoalkyl radical to Ag^+ appears much higher as that from triplet state of **DAF**. This is consistent with the potent electron donating ability of carbon-centered free radicals with adjacent nitrogen[41,42] or oxygen atom. For instance, it has been reported that ketyl radicals[43] or alkoxy benzyl radicals[22] produced photolytically are excellent reducing agents and can convert efficiently Ag^+ to Ag_0. Moreover, from the measurement of oxidation potentials of various free radicals, it has been demonstrated that α-aminoalkyl radicals are far more easily oxidized than benzyl and other arylmethyl radicals.[44,45]

The occurrence of two distinctive mechanisms of silver cations photoreduction during photopolymerization has strong consequences on the structure of the nanocomposite polymer. The TEM images relatives to each respective nanocomposite reveal important structural differences as displayed in Figure 10. The TEM image analysis of the polymer nanocomposite without MDEA indicates a broad size distribution of nanoparticles from 3 to 10 nm diameters; moreover, some areas show the presence of silver aggregates. Figure 10B is a representative TEM image of the polymer nanocomposite with MDEA, a uniform distribution of fine nanoparticles is observed with an average particles diameter on the order of 5.5 ± 0.6 nm. It can be seen that the presence of MDEA induces a uniform size dispersion of the nanoparticles, which indicates that the amine also plays an important role as capping agent (Scheme 2). Such a stabilizing role of amine systems has already been used to prevent aggregation process.[15] Moreover, the capping effect of the alkoxyamine chains should promote a better compatibility between the metal and the poly(ethylene glycol) polymer. As a consequence, this should lead to a better dispersion of the nanoparticles.

Furthermore, the morphological differences observed for these two nanocomposite polymers have a strong incidence on the fluorescence intensity of the residual chromophores which are neither engaged in the photoinitiating process nor in the photoreduction one. In Figure 11 is displayed the evolution of the relative fluorescence intensity of each sample during photopolymerization. The fluorescence intensity from the formulation with Ag^+ and MDEA undergoes a slight increase by a factor 1.6 after polymerization. However, in the case of the sample without MDEA, a larger fluorescence enhancement by a factor 6.5 is clearly observed. In all cases, the fluorescence spectra show the same emission band shape which rules out any aggregation effect (inset of Figure 11). The fluorescence

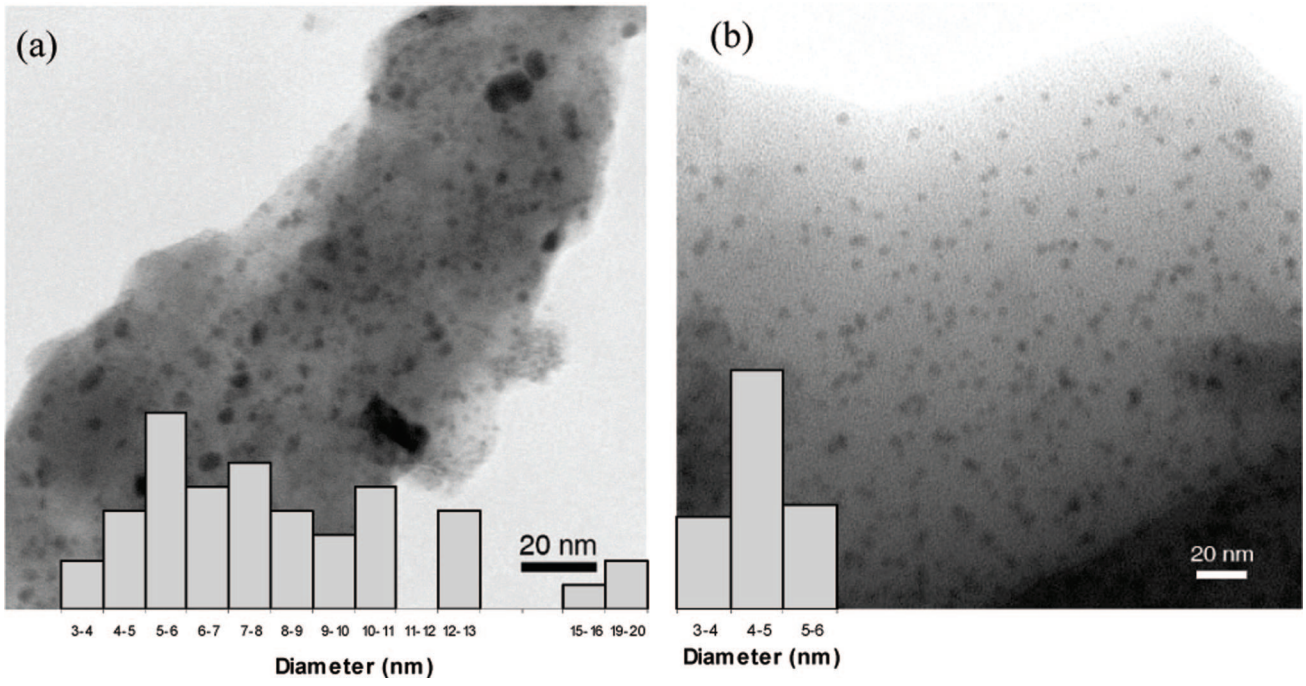

Figure 10. TEM images of silver nanoparticles embedded in polymer matrix, with their respective size distribution. (a) Formulation **DAF**/$AgNO_3$, 0.5 wt %/1 wt %. (b) Formulation **DAF**/$AgNO_3$/MDEA, 0.5 wt %/1 wt %/1 wt %.

Scheme 2. Schematic Model of the Amine Capped Silver Nanoparticle in the Poly(ethylene glycol) Matrix

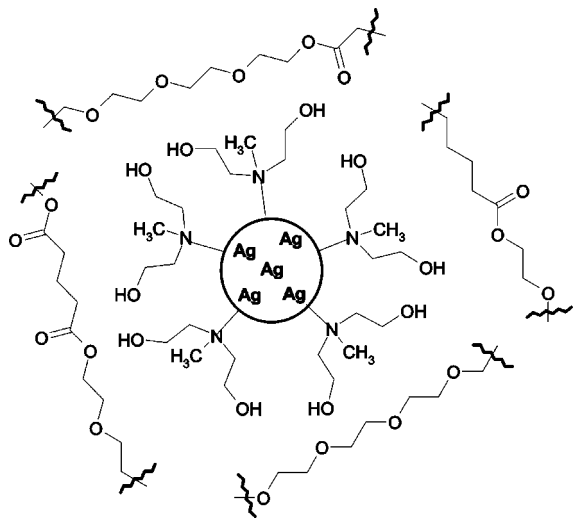

decays collected at 413 nm are confidently fitted with three exponentials. The average lifetime of the sample containing Ag^+ with MDEA has an initial value of about 2.05 ns and raises to a final value of about 4.63 ns after polymerization, whereas the sample containing Ag^+ without MDEA initially exhibits an equivalent average lifetime of about 1.97 ns but reaches a value of 2.06 ns after irradiation. All these results suggest that the radiative rate constant of chromophores entrapped in nanocomposite polymer obtained without MDEA is largely increased. This metal-enhanced fluorescence (MEF) process[46,47] should be obviously correlated to the structure of the nanocomposites. MEF is commonly observed when the distance between the fluorophore and the metallic surface is between 5−10 nm.[48] Therefore, the presence MDEA as capping agent should promote the removal of the dye from the metal surface which explains the absence of MEF for the nanocomposite polymer produced with MDEA. Moreover, MEF is also depending of the size of the silver nanoparticles, recent analysis devoted to quantify the

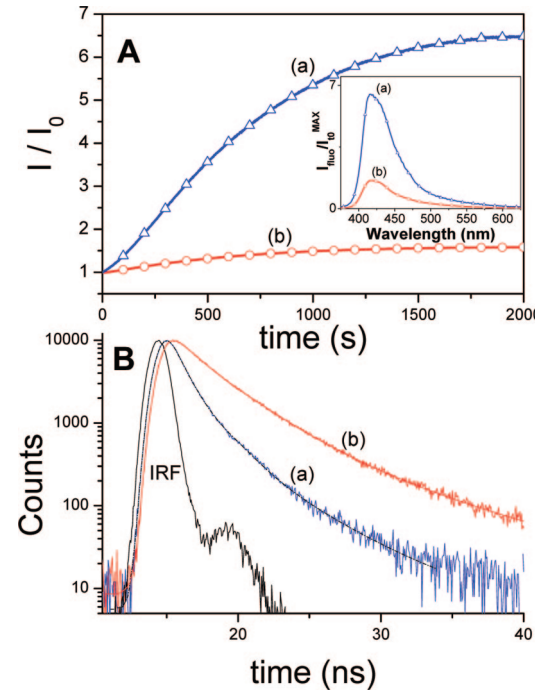

Figure 11. (A) Kinetics of the relative fluorescence intensity of formulations (λ_{em}: 413 nm) during photopolymerization (λ_{exc}: 375 nm). Inset: Final fluorescence spectra, (a) formulation **DAF**/$AgNO_3$, 0.5 wt %/1 wt %; (b) formulation **DAF**/$AgNO_3$/MDEA, 0.5 wt %/1 wt %/1 wt %. (B) Fluorescence intensity decays of nanocomposites (λ_{em}: 413 nm). The instrument response function (IRF) is included.

effects of this parameter indicates that nanoparticles with an average diameter of 50 nm leads to the most enhanced emission.[49] This is in good accordance with the presence of silver aggregates and with the broad size distribution of silver nanoparticles observed for the nanocomposite polymer produced without MDEA. Hence, from the "switch-on" emission of the dyes-embedded polymer, qualitative informations related to the silver particles growth are indirectly obtained.

Conclusion

We have investigated the photophysical properties of a 2,7-diaminofluorene derivative that both combines a photoreduction reactivity toward silver cations and a photoinitiating ability for free radical polymerization. When the dye and the silver cation are mixed together in the monomer resin, both photoreduction and photoinitiation occur parallel, without any interactions. However, the addition of a co-initiator as MDEA leads to the cross-coupling of the reactions with a new distinctive mechanism. As a consequence, the structural characteristic of nanomaterials appears clearly different. According to the stabilizing effect of MDEA, the nanocomposite polymer obtained in presence of the amine exhibits a uniform distribution of fine particles. Without MDEA, a broader size distribution is obtained which is correlated to the metal-enhanced fluorescence arising from the nonconsumed chromophores entrapped in metal−polymer nanocomposite.

References and Notes

(1) Jin, R. C.; Cao, Y. W.; Mirkin, C. A.; Kelley, K. L.; Schatz, G. C.; Zheng, J. G. *Science* **2001**, *294*, 1901.
(2) Ung, T.; Liz-Marzàn, L. M.; Mulvaney, P. *J. Phys. Chem. B* **2001**, 105.
(3) Duan, X.; Huang, Y.; Cui, Y.; Wang, J.; Lieer, C. M. *Nature* **2001**, *409*, 66–69.
(4) Holmes, J. D.; Johnston, K. P.; Doty, R. C.; Korgel, B. A. *Science* **2000**, *287*, 1471–1473.
(5) Lahav, M.; Gabriel, T.; Shipway, A. N.; Willner, I. *J. Am. Chem. Soc.* **1999**, *121* (1), 258–259.
(6) Thomas, K. G.; Kamat, P. V. *Acc. Chem. Res.* **2003**, *36*, 888–898.
(7) El-Sayed, M. A. *Acc. Chem. Res.* **2001**, *34* (4), 257–264.
(8) Eustis, S.; El-Sayed, M. A. *Chem. Soc. Rev.* **2006**, *35*, 209–217.
(9) Balan, L.; Malval, J.-P.; Schneider, R.; Burget, D. *Mater. Chem. Phys.* **2007**, *104*, 417–421.
(10) Nie, S.; Emory, S. R. *Science* **1997**, *275*, 1102–1106.
(11) Kneipp, K.; Kneipp, H.; Itskan, I.; Dasari, R. R.; Feld, M. S. *Chem. Rev.* **1999**, *99* (10), 2957–2976.
(12) Weitz, D. A.; Garoff, S.; Hansen, C. D.; Gramilla, T. J. *Opt. Lett.* **1982**, *7* (2), 89–91.
(13) Aussenegg, F.; Leitner, A.; Lippitsch, M. E.; Reinish, H.; Reigler, M. *Surf. Sci.* **1987**, *139*, 935–945.
(14) Link, S.; El-Sayed, M. A. *Int. Rev. Phys. Chem.* **2000**, *13* (3), 409–453.
(15) Kuila, B. K.; Garai, A.; Nandi, A. K. *Chem. Mater.* **2007**, *19* (22), 5443–5452.
(16) Cornelissen, J. J. L. M.; Heerbeek, R. v.; Kamer, P. C. J.; Reek, J. N. H.; Sommerdijk, N. A. J. M.; Nolte, R. J. M. *Adv. Mater.* **2002**, *14* (7), 489–492.
(17) Lim, M. H.; Ast, D. G. *Adv. Mater.* **2001**, *13* (10), 718–721.
(18) Balan, L.; Schneider, R.; Lougnot, D. J. *Prog. Org. Coat.* **2008**, *62*, 351–357.
(19) Kong, H.; Jang, J. *Chem. Commun.* **2006**, 3010–3012.
(20) Porel, S.; Singh, S.; Harsha, S. S.; Rao, D. N.; Radhakrishnan, T. P. *Chem. Mater.* **2005**, *17* (1), 9–12.
(21) Korchev, A. S.; Bozack, M. J.; Slaten, B. L.; Mills, G. *J. Am. Chem. Soc.* **2004**, *126* (1), 10–11.
(22) Sangermano, M.; Yagci, Y.; Rizza, G. *Macromolecules* **2007**, *40*, 8827–8829.
(23) Sudeep, P. K.; Kamat, P. V. *Chem. Mater.* **2005**, *17* (22), 5404–5410.
(24) Keki, S.; Torok, J.; Deak, G.; Daroczi, L.; Zsuga, M. *J. Colloid Interface Sci.* **2000**, *229*, 550–553.
(25) Meech, R.; Phillips, D. *J. Photochem.* **1983**, *23*, 193–217.
(26) Connor, D. V.; Phillips, D. *Time correlated single photon counting*; Academic Press: London, 1984.
(27) Belfield, K. D.; Bondar, M. V.; Przhonska, O. V.; Schafer, K. J. *Photochem. Photobiol. Sci.* **2004**, *3*, 138–141.
(28) Hales, J. M.; Hagan, D. J.; Stryland, E. W. V.; Schafer, K. J.; Morales, A. R.; Belfield, K. D.; Pacher, P.; Kwon, O.; Zojer, E.; Bredas, J. L. *J. Chem. Phys.* **2004**, *121* (7), 3152–3160.
(29) Belfield, K. D.; Bondar, M. V.; Przhonska, O. V.; Schafer, K. J.; Mourad, W. *J. Lumin.* **2002**, *97*, 141–146.
(30) Sumalekshmy, S.; Gopidas, K. R. *Chem. Phys. Lett.* **2005**, *413*, 294–299.
(31) Kirchgessner, M.; Sreenath, K.; Gopidas, K. R. *J. Org. Chem.* **2006**, *71*, 9849–9852.
(32) Martineau, C.; Anémian, R.; Andraud, C.; Wang, I.; Bouriau, M.; Baldeck, P. L. *Chem. Phys. Lett.* **2002**, *362*, 291–295.
(33) Jönsson, S.; Viswanathan, K.; Hoyle, C. E.; Clark, S. C.; Miller, C.; Nguyen, C.; Zhao, W.; Shao, L.; Morel, F.; Decker, C. *J. Photopolym. Sci. Technol.* **2000**, *13* (1), 125–144.
(34) Bibaut-Renauld, C.; Burget, D.; Fouassier, J. P.; Varelas, C. G.; Thomatos, J.; Tsagaropoulos, G.; Ryrfors, L. O.; Karlsson, O. J. *J. Polym. Sci., Part A: Polym. Chem.* **2002**, *40*, 3171–3181.
(35) Dickens, S. H.; Stansbury, J. W.; Choi, K. M.; Floyd, C. J. E. *Macromolecules* **2003**, *36*, 6043–6053.
(36) Andrzejewska, E.; Linden, L. A.; Rabek, J. F. *Macromol. Chem. Phys.* **1998**, *199*, 441–449.
(37) Handoo, K. L.; Cheng, J.-P.; Parker, V. D. *J. Chem. Soc., Perkin Trans. 2* **2001**, *1476*, 1480.
(38) Knolle, W.; Janovsky, I.; Naumov, S.; Williams, F. *J. Phys. Chem. A* **2006**, *110* (51), 13816–13826.
(39) Fischer, H.; Radom, L. *Angew. Chem., Int. Ed.* **2001**, *40*, 1340–1371.
(40) Wu, J. Q.; Beranek, I.; Fischer, H. *Helv. Chim. Acta* **1995**, *78*, 194.
(41) Eksik, O.; Erciyes, A. T.; Yagci, Y. *J. Macromol. Sci., Part A: Pure Appl. Chem.* **2008**, *45*, 698–704.
(42) Kim, J. Y.; Shin, D. H.; Ihn, K. J. *Macromol. Chem. Phys.* **2005**, *206*, 794–801.
(43) Scaiano, J. C.; Aliaga, C.; Maguire, S.; Wang, D. *J. Phys. Chem. B* **2006**, *110* (26), 12856–12859.
(44) Wayner, D. D. M.; Dannenberg, J. J.; Griller, D. *Chem. Phys. Lett.* **1986**, *131* (3), 189–191.
(45) Wayner, D. D. M.; Griller, D. *J. Am. Chem. Soc.* **1985**, *107*, 7764–7765.
(46) Geddes, C. D.; Cao, H.; Gryczynski, I.; Gryczynski, Z.; Fang, J.; Lakowicz, J. R. *J. Phys. Chem. A* **2003**, *107* (18), 3443–3449.
(47) Parfenov, A.; Gryczynski, I.; Malicka, J.; Geddes, C. D.; Lakowicz, J. R. *J. Phys. Chem. B* **2003**, *107* (34), 8829–8833.
(48) Lakowicz, J. R.; Geddes, C. D.; Gryczynski, I.; Malicka, J.; Gryczynski, Z.; Aslan, K.; Lukomska, J.; Matveeva, E.; Zhang, J.; Badugu, R.; Huang, J. *J. Fluoresc.* **2004**, *14* (4), 425–441.
(49) Zhang, J.; Fu, Y.; Chowdhury, M. H.; Lakowicz, J. R. *J. Phys. Chem. C* **2007**, *112* (1), 18–26.

MA8017926